

# Prograde and Retrograde Black Holes: Whose Jet is More Powerful?

Alexander Tchekhovskoy<sup>1\*</sup> and Jonathan C. McKinney<sup>2</sup>

<sup>1</sup>Center for Theoretical Science, Jadwin Hall, Princeton University, Princeton, NJ 08544; Princeton Center for Theoretical Science Fellow

<sup>2</sup>Kavli Institute for Particle Astrophysics and Cosmology, Stanford University, P.O. Box 20450, MS 29, Stanford, CA 94309

Accepted . Received ; in original form

## ABSTRACT

The outflow efficiency ( $\eta$ ) from black hole (BH) accretion disc systems is known to depend upon both the BH spin ( $a$ ) and the amount of large-scale magnetic flux threading the BH and disc. Semi-analytical flux-trapping models suggest retrograde BHs should trap much more large-scale magnetic flux near the BH leading to much higher  $\eta$  than for prograde BHs. We self-consistently determine the amount of large-scale magnetic flux trapped by rapidly spinning ( $a = -0.9$  and  $0.9$ ) BHs using global 3D time-dependent non-radiative general relativistic magnetohydrodynamic simulations of thick ( $h/r \approx 0.3-0.6$ ) discs. We find that BH-trapped flux builds up until it is strong enough to disrupt the inner accretion disc. Contrary to prior flux-trapping models, which do not include the back-reaction of magnetic flux on the disc, our simulations show prograde BHs trap more magnetic flux, leading to about 3 times higher  $\eta$  than retrograde BHs for  $|a| = 0.9$ . Both spin orientations can produce highly efficient jets,  $\eta \sim 100\%$ , with increasing  $\eta$  for increasing disc thickness. The similarity of  $\eta$  for prograde and retrograde BHs makes it challenging to infer the sign of  $a$  based on jet energetics alone.

**Key words:** black hole physics — (magnetohydrodynamics) MHD — accretion, accretion discs — galaxies: jets — gamma-rays: bursts — methods: numerical

## 1 INTRODUCTION

Various astrophysical systems—active galactic nuclei (AGN), black hole binaries (BHBs), and gamma-ray bursts (GRBs)—produce relativistic outflows. Mediated by large scale magnetic fields, outflows can be powered by the central BHs via Blandford & Znajek (1977, BZ hereafter) mechanism or by the inner regions of accretion discs via Blandford & Payne (1982, BP hereafter) mechanism.

Large-scale magnetic fields extract BH spin energy at a rate,

$$P_{\text{BZ}} = \frac{\kappa}{4\pi c} \Phi_{\text{BH}}^2 \Omega_{\text{H}}^2 f(\Omega_{\text{H}}), \quad (1)$$

where  $\kappa \approx 0.05$  weakly depends on field geometry,  $\Phi_{\text{BH}} = (1/2) \iint_{\theta, \varphi} |B^r| dA_{\theta\varphi}$  is an absolute magnetic flux through the BH, with the integral over all  $\theta$  and  $\varphi$  on the BH horizon,  $r_{\text{H}} = r_g(1 + \sqrt{1 - a^2})$ . Here  $r_g = GM/c^2$ ,  $M$ , and  $a$  are BH gravitational radius, mass, and dimensionless spin,  $\Omega_{\text{H}} = ac/2r_{\text{H}}$  is BH angular frequency,  $f(\Omega_{\text{H}}) \approx 1 + 1.38(\Omega_{\text{H}}r_g/c)^2 - 9.2(\Omega_{\text{H}}r_g/c)^4$  is a high-spin correction,  $dA_{\theta\varphi} = \sqrt{-g} d\theta d\varphi$  is an area element in  $\theta - \varphi$  plane, and  $g$  is the metric determinant (Tchekhovskoy et al. 2010, see also BZ; Lee et al. 2000; Komissarov 2001; Tanabe & Nagataki 2008).

For fixed  $\Phi_{\text{BH}}$ ,  $P_{\text{BZ}}$  is the same for prograde ( $a > 0$ ) and retrograde ( $a < 0$ ) BHs. However, a massive accretion disc introduces a preferred spin/rotation direction. Does this lead to large differences in  $\Phi_{\text{BH}}$  and jet powers of prograde and retrograde BHs? Under-

standing this is crucial, as the link between jet power and BH spin has been confirmed in BHBs (Narayan & McClintock 2012, but see Fender et al. 2010) and jet power is increasingly often used for inferring BH spin (Daly 2011; Martínez-Sansigre & Rawlings 2011; Buliga et al. 2011; Lei & Zhang 2011; Bambi 2012).

To quantify jet strength in an accretion system, we define BZ efficiency as jet power (eq. 1) in units of mass accretion rate,  $\dot{M}$ ,

$$\eta_{\text{BZ}} = \frac{P_{\text{BZ}}}{\langle \dot{M} \rangle c^2} \times 100\% = \frac{\kappa}{4\pi} \phi_{\text{BH}}^2 \left( \frac{\Omega_{\text{H}} r_g}{c} \right)^2 f(\Omega_{\text{H}}) \times 100\%, \quad (2)$$

where  $\phi_{\text{BH}} = \Phi_{\text{BH}} / (\langle \dot{M} \rangle r_g^2 c)^{1/2}$  is BH dimensionless magnetic flux, and  $\langle \dots \rangle$  is a time average. Similarly, we define magnetic flux enclosed by a toroidal ring,  $(r, \theta)$ , via  $\Phi(r, \theta) = \iint_{\theta' < \theta, \varphi'} B^r dA_{\theta'\varphi'}$ , and its dimensionless version,  $\phi(r, \theta) = \Phi(r, \theta) / (\langle \dot{M} \rangle r_g^2 c)^{1/2}$ , where the integral is over a polar cap,  $\theta' < \theta$ , of a sphere of radius  $r$ .

Clearly, jet efficiency depends on the ability of accretion flows to drag large-scale magnetic fields to the centre. Lubow et al. (1994) studied magnetic field dragging by geometrically thin accretion discs, with angular thickness,  $h/r \ll 1$ . They found that field transport is governed by the value of the magnetic Prandtl number ( $\text{Pr}_{\text{m}}$ , which is the ratio of turbulent viscosity to resistivity) and that in order for field dragging to be efficient, this number must be large,  $\text{Pr}_{\text{m}} \gtrsim (h/r)^{-1} \gg 1$ . Magneto-rotational instability (MRI, Balbus & Hawley 1991) driven turbulent accretion flows have low values of magnetic Prandtl number,  $\text{Pr}_{\text{m}} \sim 1$  (Fromang & Stone 2009; Guan & Gammie 2009; Lesur & Longaretti 2009). For such natural

\* E-mail: atchekho@princeton.edu (AT)

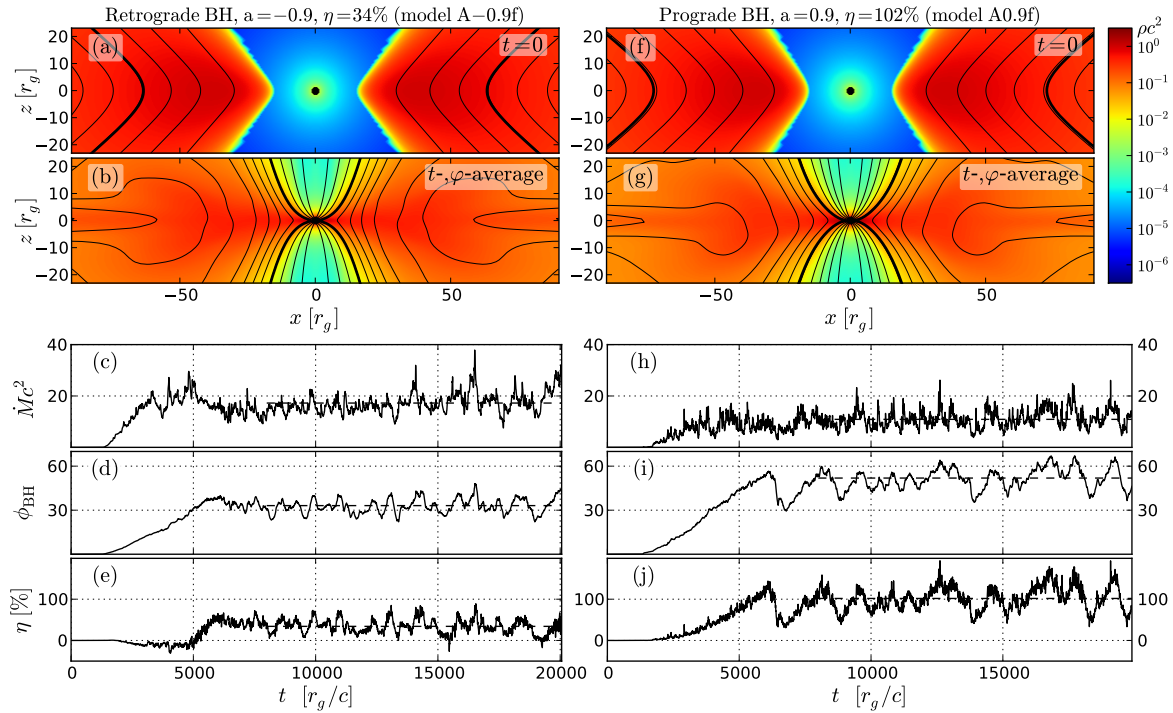


**Figure 1.** Initial conditions and time-evolution of our fiducial models, A–0.9f (left column) and A0.9f (right column). See Supporting Information for movies. [Panels a,f] A vertical slice through the initial conditions. Colour shows fluid frame rest-mass energy density (see colour bar) and thin black lines show levels of constancy of enclosed magnetic flux,  $\langle\Phi\rangle$ , which represent field lines in the image plane. Magnetic field is axisymmetric, with  $B_\varphi = 0$  everywhere and  $B_z > 0$  out to few  $\times 100r_g$ . Only the magnetic flux enclosed by the thick solid field line eventually falls into the BH. [Panels b,g] Show  $t$ - and  $\varphi$ -average of the magnetically-arrested state of the simulation. Solid lines show the same contours of  $\langle\Phi\rangle$  as in panels (a) and (f). Accretion accumulates so much flux in the centre that the inner disc is able to push only a fraction of the flux, enclosed by the thick line, into the BH. [Panels c-e,h-j] From top to bottom: rest-mass energy accretion rate,  $\dot{M}c^2$ , dimensionless BH magnetic flux,  $\phi_{\text{BH}}$ , and energy outflow efficiency,  $\eta$ . Both  $\phi_{\text{BH}}$  and  $\eta$  saturate at  $t \gtrsim 6000r_g/c$ , beyond which the accretion flow is magnetically arrested. Dashed lines show time-averages: a prograde BH has a larger efficiency,  $\eta = 102\%$ , than a retrograde BH,  $\eta = 34\%$ .

values,  $\text{Pr}_m \sim 1$ , thin discs do not produce centrally-concentrated magnetic fields, which suggests that thin discs produce weak or no jets (Lubow et al. 1994; but see Spruit & Uzdensky 2005; Rothstein & Lovelace 2008). To include general-relativistic (GR) effects of the innermost stable circular orbit (ISCO) on field dragging in thin discs, Reynolds et al. (2006) proposed that gas and fields plunge into the BH inside the ISCO, so no magnetic flux passes through the “gap” between the BH horizon and the ISCO. Based on a GR-version of this flux-trapping “gap” model, formally applicable only to thin discs, Garofalo (2009); Garofalo et al. (2010) concluded that jets from retrograde BHs,  $a = -0.9$ , are  $\gtrsim 10\times$  more powerful than from prograde BHs,  $a = 0.9$ , both for thin and thick discs (see §2).

Geometrically thick discs can efficiently drag large-scale fields inward even for  $\text{Pr}_m \sim 1$  (Cao 2011), and time-dependent simulations of McKinney & Gammie (2004); McKinney (2005); Hawley & Krolik (2006) show that thick accretion discs ( $h/r \simeq 0.2\text{--}0.3$ ) can produce powerful jets. However, the simulated values of jet efficiency have a high degree of scatter, e.g., jet efficiency from retrograde BHs ranges in these works from 10% to 50% of the corresponding efficiency for prograde BHs at the same absolute value of spin. A major uncertainty in such studies is the dependence of jet efficiency on the value of large-scale vertical magnetic flux initially present in the disc, which is a free modeling parameter with no obvious natural value. Changes in the flux can significantly affect simulated jet efficiencies (McKinney & Gammie 2004; McKinney 2005; Beckwith et al. 2008) and render them unreliable.

Is it at all possible to obtain a well-defined value of jet efficiency, free from the uncertainties in large-scale magnetic flux

content of the initial simulation setup? Tchekhovskoy et al. (2011, TNM11 hereafter) showed that a promising approach is to start with a large vertical magnetic flux in the disc, more than the accreting gas can push into the BH. The excess flux remains outside, impedes the accretion, and leads to a magnetically-arrested disc (MAD, Bisnovatyi-Kogan & Ruzmaikin 1974; Narayan et al. 2003; Igumenshchev et al. 2003; Igumenshchev 2008; TNM11). Estimates show that many astrophysical systems contain enough large-scale magnetic flux to naturally form MADs (Narayan et al. 2003; McKinney et al. 2012). The inner disc properties of MADs are shown to be *independent of the initial value of large-scale magnetic flux*. So, we can reliably determine  $\eta$  for prograde and retrograde BHs and thereby test the flux-trapping “gap” model. In §2 we describe our numerical method and present our results and in §3 we conclude.

## 2 NUMERICAL METHOD AND RESULTS

We carried out time-dependent 3D general relativistic non-radiative MHD simulations using a high-order version of Godunov-type shock-capturing code HARM (Gammie et al. 2003; McKinney & Gammie 2004; Tchekhovskoy et al. 2007, 2009; McKinney & Blandford 2009) in modified spherical polar coordinates. We use logarithmically spaced radial grid,  $dr/r = \text{constant}$ , for  $r \lesssim r_{\text{br}}$  (see Table 1 for  $r_{\text{br}}$  values). For  $r \gtrsim r_{\text{br}}$ , the grid becomes progressively sparser,  $dr/r = 4(\log r)^{3/4}$ , with a smooth transition at  $r_{\text{br}}$ . We choose grid inner radius,  $R_{\text{in}}$ , such that there are at least 9 grid cells between the inner radial boundary and the BH horizon and place

**Table 1.** Simulation details

Name <sup>a</sup>	$a$	$\eta^b$ [%]	$\beta_{\min}$	$\Delta\varphi$	Resolution <sup>c</sup>	$r_{\text{in}}/r_g$	$r_{\text{max}}/r_g$	$R_{\text{in}}/r_{\text{H}}$	$R_{\text{out}}/r_g$	$r_{\text{br}}/r_g$	$t_{\text{run}} [r_g/c]$	$t_{\text{avg}} [r_g/c]$
Simulations with $(h/r)_{r_{\text{max}}} \approx 0.2$ and $\langle h/r \rangle_{30} \approx 0.3$ :												
A-0.9f	-0.9	$34 \pm 3$	100	$2\pi$	$288 \times 128 \times 64$	15	37.1	0.7	$10^5$	$10^3$	(0; 20060)	(8000; 20060)
A-0.9	-0.9	$43 \pm 8$	100	$\pi$	$288 \times 128 \times 32$	15	37.1	0.8	$10^5$	$10^2$	(0; 16535)	(8000; 16535)
A-0.9 $l_r$	-0.9	$45 \pm 8$	100	$\pi$	$144 \times 128 \times 32$	15	37.1	0.8	$10^5$	$10^2$	(0; 18760)	(8000; 18760)
A-0.9 $l_\theta$	-0.9	$41 \pm 4$	100	$\pi$	$288 \times 64 \times 32$	15	37.1	0.8	$10^5$	$10^2$	(0; 17570)	(8000; 17570)
A-0.9 $h_\theta$	-0.9	$40 \pm 5$	100	$\pi$	$288 \times 256 \times 32$	15	37.1	0.8	$10^5$	$10^2$	(12328; 16535)	(12328; 16535)
A-0.9 $h_\varphi$	-0.9	$36 \pm 5$	100	$\pi$	$288 \times 128 \times 64$	15	37.1	0.8	$10^5$	$10^2$	(8000; 14745)	(8000; 14745)
A-0.9flip	-0.9	$40 \pm 8$	100	$\pi$	$288 \times 128 \times 32$	15	34.1	0.8	$10^5$	$10^2$	(14207; 18790)	(14207; 18790)
A0.9f	0.9	$102 \pm 10$	100	$2\pi$	$288 \times 128 \times 64$	15	34.1	0.8	$10^5$	$10^2$	(0; 19895)	(8000; 19895)
A0.9	0.9	$96 \pm 17$	100	$\pi$	$288 \times 128 \times 32$	15	34.1	0.8	$10^5$	$10^2$	(0; 22285)	(8000; 22285)
A0.9 $l_r$	0.9	$113 \pm 13$	100	$\pi$	$144 \times 128 \times 32$	15	34.1	0.57	$10^5$	$10^2$	(0; 20350)	(8000; 20350)
A0.9 $h_r$	0.9	$115 \pm 20$	100	$\pi$	$576 \times 128 \times 32$	15	34.1	0.8	$10^5$	$10^2$	(0; 16265)	(8000; 16265)
A0.9 $l_\theta$	0.9	$97 \pm 14$	100	$\pi$	$288 \times 64 \times 32$	15	34.1	0.8	$10^5$	$10^2$	(0; 16915)	(8000; 16915)
A0.9 $h_\theta$	0.9	$123 \pm 22$	100	$\pi$	$288 \times 256 \times 32$	15	34.1	0.8	$10^5$	$10^2$	(14207; 22290)	(14207; 22290)
A0.9 $h_\theta h_\varphi$	0.9	$112 \pm 19$	100	$\pi$	$288 \times 256 \times 64$	15	34.1	0.8	$10^5$	$10^2$	(14207; 24410)	(14207; 24410)
A0.9 $h_\varphi$	0.9	$109 \pm 21$	100	$\pi$	$288 \times 128 \times 64$	15	34.1	0.8	$10^5$	$10^2$	(0; 15550)	(8000; 15550)
A0.9 $h_\varphi^2$	0.9	$103 \pm 14$	100	$\pi$	$288 \times 128 \times 128$	15	34.1	0.8	$10^5$	$10^2$	(8500; 14625)	(8500; 14625)
A0.9N25	0.9	$116 \pm 32$	25	$\pi$	$288 \times 128 \times 32$	15	34.1	0.8	$10^5$	$10^2$	(0; 17350)	(8000; 17350)
A0.9N50	0.9	$114 \pm 20$	50	$\pi$	$288 \times 128 \times 32$	15	34.1	0.8	$10^5$	$10^2$	(0; 14385)	(8000; 14385)
A0.9N200	0.9	$118 \pm 32$	200	$\pi$	$288 \times 128 \times 32$	15	34.1	0.8	$10^5$	$10^2$	(0; 28620)	(16000; 28620)
A0.9R20	0.9	$102 \pm 19$	100	$\pi$	$288 \times 128 \times 32$	20	45.35	0.8	$10^5$	$10^2$	(0; 15295)	(8000; 15295)
Simulations with $(h/r)_{r_{\text{max}}} \approx 0.6$ and $\langle h/r \rangle_{30} \approx 0.6$ :												
A-0.94BfN30	-0.9375	$88 \pm 75$	30	$2\pi$	$136 \times 64 \times 128$	10	100	0.73	26000	500	(0; 13000)	(8000; 13000)
A0.94BfN30	0.9375	$354 \pm 43$	30	$2\pi$	$136 \times 64 \times 128$	10	100	0.73	26000	500	(0; 13000)	(8000; 13000)

<sup>a</sup> Suffixes “ $h_\theta$ ” or “ $l_\theta$ ” indicate that  $\theta$ -resolution was increased or, respectively, decreased by a factor of two as compared to the fiducial model. Models A0.9 $l_\theta$ , A0.9 $h_\theta$ , and A0.9 $h_\theta h_\varphi$  are similar to model A0.9 but with  $\theta$ - and  $\varphi$ -resolutions increased by factors  $f_\theta$  and  $f_\varphi$ , respectively, at  $t = 14207r_g/c$ , where the pairs of values,  $(f_\theta, f_\varphi)$ , are given by (0.5, 1), (2, 1), and (2, 2), respectively. Model A-0.9flip is similar to model A0.9, but with BH spin value reversed to  $a = -0.9$  at  $t = 14207r_g/c$ . Model A-0.9 $h_\theta$  (A-0.9 $h_\varphi$ ) is similar to model A-0.9 but with  $\theta$ -resolution ( $\varphi$ -resolution) increased by a factor of two at  $t = 12328r_g/c$  (at  $t = 8000r_g/c$ , respectively). Model A0.9 $h_\varphi^2$  is similar to model A0.9 $h_\varphi$  but with  $\varphi$ -resolution increased by a factor of two at  $t = 8500r_g/c$ .

<sup>b</sup> We quote 95.4% (two sigma) confidence intervals. <sup>c</sup> Given as  $N_r \times N_\theta \times N_\varphi$ , where  $N_r$ ,  $N_\theta$ , and  $N_\varphi$  are grid resolutions in  $r$ -,  $\theta$ -, and  $\varphi$ -directions, respectively.

the outer radial boundary at  $R_{\text{out}} = 10^5 r_g$ , which is larger than the light travel distance in a duration of the simulation (see Table 1 for  $R_{\text{in}}$  values). This ensures that both radial boundaries are causally disconnected. We use standard boundary conditions (see TNM11): outflow in  $r$ -, reflecting in  $\theta$ -, and periodic in  $\varphi$ -directions.

We consider a retrograde fiducial model, A-0.9f, for spin  $a = -0.9$ , and a prograde fiducial model, A0.9f, for spin  $a = 0.9$ . Figure 1(a),(f) shows our initial conditions: BH at the centre of an equilibrium hydrodynamic torus (Chakrabarti 1985; De Villiers & Hawley 2003), with angular velocity,  $\Omega \propto r^{-1.75}$ . We place the torus inner edge at  $r_{\text{in}} = 15r_g$  and pressure maximum at  $r_{\text{max}} \sim 35r_g$ , so disc angular thickness at  $r_{\text{max}}$  is  $(h/r)_{r_{\text{max}}} \approx 0.2$  (see Table 1). Here  $(h/r)_r = \left[ \iint_{\theta, \varphi} (\theta - \pi/2)^2 \rho dA_{\theta\varphi} / \iint_{\theta, \varphi} \rho dA_{\theta\varphi} \right]^{1/2}$  and the integral is over all  $\theta, \varphi$  on a sphere of radius  $r$ . We embed the torus with a purely poloidal ( $B_\varphi = 0$ ) loop of a weak magnetic field, with plasma  $\beta \equiv p_{\text{gas}}/p_{\text{mag}} \geq \beta_{\min} = 100$ . The loop contains a large magnetic flux due to the large radial extent of the loop (see TNM11).

We define rates of accretion of rest mass,  $\dot{M}$ , and rest mass energy,  $F_M \equiv \dot{M}c^2$ , by  $\dot{M} = -\iint_{\theta, \varphi} \rho u^r dA_{\theta\varphi} \equiv F_M/c^2 > 0$ , where  $\rho$  is fluid-frame mass density,  $u^r$  is  $r$ -component of contravariant 4-velocity, and the integration is over all  $\theta, \varphi$  on the BH horizon,  $r = r_{\text{H}}$ . Figure 1(c),(h) shows that after the start of the simulation  $\dot{M}$  settles to a steady state at  $t \gtrsim 5000r_g/c$ . BH magnetic flux,  $\phi_{\text{BH}}$ , increases until  $t \sim 6000r_g/c$ , beyond which  $\phi_{\text{BH}}$  saturates (Figure 1d,i). Flux accumulates outside the BH, impedes the accretion, and leads to a magnetically-arrested accretion disc (MAD, Narayan et al. 2003). Some of the BH flux occasionally escapes from the BH

via magnetic interchange (Stehle & Spruit 2001; TNM11), leading to oscillations of  $\phi_{\text{BH}}$  in time (Fig. 1d,i). Figure 1(b),(g) shows the  $t$ - and  $\varphi$ -average of the flow over the MAD period ( $t_{\text{avg}}$  in Table 1). In order to get to the BH, gas “diffuses” through the vertical magnetic flux that reached size  $\sim 25r_g$  in a duration of our simulations. At large  $r \gtrsim 30r_g$ , all our discs have very similar values of angular thickness,  $\langle h/r \rangle_{30} \approx 0.3$  (see Table 1). At smaller  $r$ , funnel magnetic fields compress the disc vertically and lead to smaller  $h/r$ .

We define total energy accretion rate (as measured at infinity),  $F_E = \iint_{\theta, \varphi} T^r_t dA_{\theta\varphi}$ , where  $T^{\mu}_\nu$  is stress-energy tensor, the integral is over all  $\theta, \varphi$  on BH horizon, and  $F_E$  is positive if energy flows into the BH. We define energy outflow efficiency  $\eta$  as the energy return rate to infinity divided by the time-average mass accretion rate:

$$\eta \equiv \frac{F_M - F_E}{\langle F_M \rangle} \times 100\%. \quad (3)$$

Time-dependence of  $\eta$  for our fiducial models, A-0.9f and A0.9f, is shown in Figure 1(e),(j). The outflow efficiency saturates at  $t \gtrsim 6000r_g/c$  and clearly correlates with  $\phi_{\text{BH}}$ . This is not surprising since we will see below that most of the outflowing energy is carried by BZ-driven jets, hence  $\eta \approx \eta_{\text{BZ}} \propto \phi_{\text{BH}}^2$  (eq. 2). A retrograde BH traps  $\approx 30$  units of  $\phi_{\text{BH}}$  (panel d), while a prograde BH traps  $\approx 50$  units (panel i). Correspondingly, the retrograde BH produces outflows  $(50/30)^2 \approx 3$  times less efficiently (see eq. 2), with  $\eta = 34 \pm 3\%$  (panel e), than the prograde BH, which has  $\eta = 102 \pm 10\%$  (panel j and Table 1). It is interesting to compare these results to those for thicker discs,  $\langle h/r \rangle_{30} \approx 0.6$ , and a some-

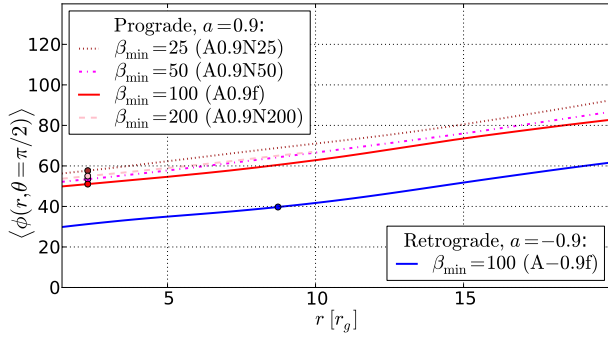


**Figure 2.** Equatorial profile of magnetic flux,  $\langle \phi(r, \theta = \pi/2) \rangle$ , in models different by the initial amount of large-scale magnetic flux (see legend). The ISCO radius is indicated by filled circles. Despite the magnetic flux content of the models varying by a factor of  $\approx 3$ , all prograde models (top cluster of curves) agree to  $\lesssim 10\%$ . Hence, flux accumulation around the centre in our simulations is independent of the initial large-scale flux content of the disc.

what larger magnitude of BH spin,  $|a| = 0.9375$ . The retrograde model has  $\eta = 88 \pm 75\%$  and the prograde model has  $\eta = 354 \pm 43\%$  (see Table 1 and McKinney et al. 2012). Thicker discs reach higher  $\eta$ , and prograde BHs have higher  $\eta$  than retrograde BHs.

We repeated our fiducial models in a reduced azimuthal wedge,  $\Delta\varphi = \pi$ . We refer to them as A-0.9 and A0.9 and find  $\eta = 43 \pm 8\%$  and  $\eta = 96 \pm 17\%$ , respectively, in agreement with our fiducial models. We carried out a number of resolution studies (see Table 1) and find they agree with our fiducial models within  $\eta$  measurement uncertainty (see Table 1): the mean efficiency of our retrograde models is  $\eta = 38 \pm 4\%$  and of prograde models is  $\eta = 106 \pm 7\%$ . Hence,  $\eta$  values are converged in our fiducial models, which at  $r = 10r_g$  have  $Q_z \approx 95$  and  $Q_\varphi \approx 20$  cells per the fastest growing  $z$ - and  $\varphi$ -MRI wavelengths, respectively, and an equatorial cell aspect ratio,  $\delta r : r\delta\theta : r\delta\varphi \approx 2 : 1 : 7$ . Our highest  $\varphi$ -resolution model, A0.9 $h_\varphi^2$ , has  $Q_z \approx Q_\varphi \approx 100$  and  $\delta r : r\delta\theta : r\delta\varphi \approx 2 : 1 : 2$  and is very well resolved according to MRI resolution criteria (e.g., Hawley et al. 2011; Sorathia et al. 2011).

Why do outflow efficiencies of prograde and retrograde BHs differ? Can this be due to differences in initial conditions amplified by accretion flow turbulence? To test this, we ran the prograde model A0.9 until  $t = 14207r_g/c$  and instantaneously flipped the direction of BH spin. We refer to this model as A-0.9flip, which gives  $\eta = 40 \pm 8\%$ , consistent with our previous retrograde results. But what about large-scale magnetic flux? Since its value is conserved, the differences in the flux cannot be erased by turbulence; can they affect the outcome? To test this, we carried out a series of simulations different only by the magnitude of the magnetic field, i.e., with  $\beta_{\min} = \{25, 50, 100, 200\}$ . We refer to these simulations as models A0.9N25, A0.9N50, A0.9f (our fiducial prograde model), A0.9N200, respectively. The initial fluxes in these models differ by a factor of  $\approx 3$ . Does this lead to a similar difference in the magnetic flux that reaches the BH? Figure 2 shows that all models have equatorial magnetic flux profiles,  $\langle \phi(r, \theta = \pi/2) \rangle$ , that agree to  $\lesssim 10\%$ , and  $\eta$  that agree to  $\lesssim 20\%$  (see Table 1). This demonstrates that  $\phi_{\text{BH}}$  and  $\eta$  are *independent of the initial magnetic flux content* of the flow. We also verified that our results are insensitive to the initial position of the torus (see model A0.9R20 in Table 1).

So far we considered the total energy output of the BH. What fraction of this energy goes into jets and into winds? The  $t$ - and  $\varphi$ -averages of our fiducial models, A-0.9f and A0.9f, shown in Figure 3, have similar hourglass shapes. The equatorial part of the accretion flow directly reaches the BH, while the inflow at higher lati-

tudes turns around and forms weakly magnetized disc winds. These winds confine the highly magnetized relativistic polar jets that directly connect to the BH. Figure 3(a) shows that in the retrograde model, A-0.9f, the efficiency of the wind is  $\eta_{\text{wind}}(-0.9) \approx 7\%$ . The remainder comprises jet efficiency,  $\eta_{\text{jet}}(-0.9) \approx 34 - 7 = 27\%$ . Similarly, Figure 3(b) shows that wind efficiency for the prograde model, A0.9f, is  $\eta_{\text{wind}}(0.9) \approx 16\%$ , so jet efficiency is  $\eta_{\text{jet}}(0.9) \approx 102 - 16 = 86\%$ . In both cases, the jet, which is predominantly powered by the BZ mechanism, carries most ( $\approx 80\%$ ) of the total power output, and the power of the wind, launched by a BP-like mechanism, is subdominant. Note that all energy flow streamlines start on the BH and none start in the body of the disc. This is a manifestation of energy conservation: energy can either come from the BH via the release of gravitational binding energy or Penrose/BZ effect, or it can be advected inward from large distances by accreting material (if the accretion flow is unbound at large radii).

Our results differ from semi-analytical flux-trapping “gap” models (Garofalo 2009), which predict for  $|a| = 0.9$  that retrograde BHs produce  $\gtrsim 10\times$  more powerful jets than prograde BHs. The “gap” models make use of a sharp transition at the ISCO to a plunge flow that sweeps into the BH all flux from an area (the “gap”) between the BH horizon and the ISCO. Since retrograde BHs have the largest ISCO area, in the “gap” model they receive the largest flux and produce the most powerful jets. However, poloidal flux distributions in our prograde and retrograde simulations are strikingly similar and show no “gap” (see Figures 2, 3): clearly, the “gap” model does not apply to thick radiatively-inefficient discs (unlike used by Garofalo 2009; Garofalo et al. 2010). This is not surprising because the sharp transition to the plunge at the ISCO, which the “gap” model relies on, is pronounced only for very thin ( $h/r \lesssim 0.05$ ) radiatively-efficient discs (Penna et al. 2010). In addition, a key piece of physics is missing from flux-trapping “gap” models: “gap” models assume that magnetic field is weak and has no back-reaction on the plunging inflow. However, BH magnetic flux builds up to a natural saturation point at which the field does back-react: the magnetic flux not only modifies the rotation rate of plasma in the plunging region, it also escapes from the BH via magnetic interchange (Stehle & Spruit 2001; TNM11; McKinney et al. 2012). In our simulations, this non-axisymmetric mechanism fills-in the ISCO region with magnetic flux. No “gap” forms because the inflow of magnetic flux happens just as fast as the outflow of magnetic flux, unlike in the flux-trapping “gap” models. “Gap” models have not yet accounted for these effects, which dominate in MADs and, hence, in accretion systems with the most efficient jets.

### 3 CONCLUSIONS

We set out to determine whether prograde or retrograde BHs produce the most efficient outflows. Accretion discs with large-scale vertical magnetic fields naturally evolve into a magnetically-arrested disc (MAD) state in which the central BH is saturated with magnetic flux and the outflow efficiency ( $\eta$ ) is *maximum*. Our simulations show that in this state,  $\eta$  only depends on the BH spin,  $a$ , and the angular thickness of the accretion disc,  $h/r$ , and is *independent of the initial magnetic flux* content of the disc (see §2).

We find that for medium-thickness discs,  $h/r \approx 0.3$ , and an absolute value of spin,  $|a| = 0.9$ , a retrograde BH produces jets and winds with an efficiency,  $\eta = 38 \pm 4\%$ , which is a few times smaller than a prograde BH,  $\eta = 106 \pm 7\%$ . In both cases, most of the energy ( $\approx 80\%$ ) emerges in the form of BZ-powered, relativistic, highly magnetized collimated polar jets (see §2). We expect the

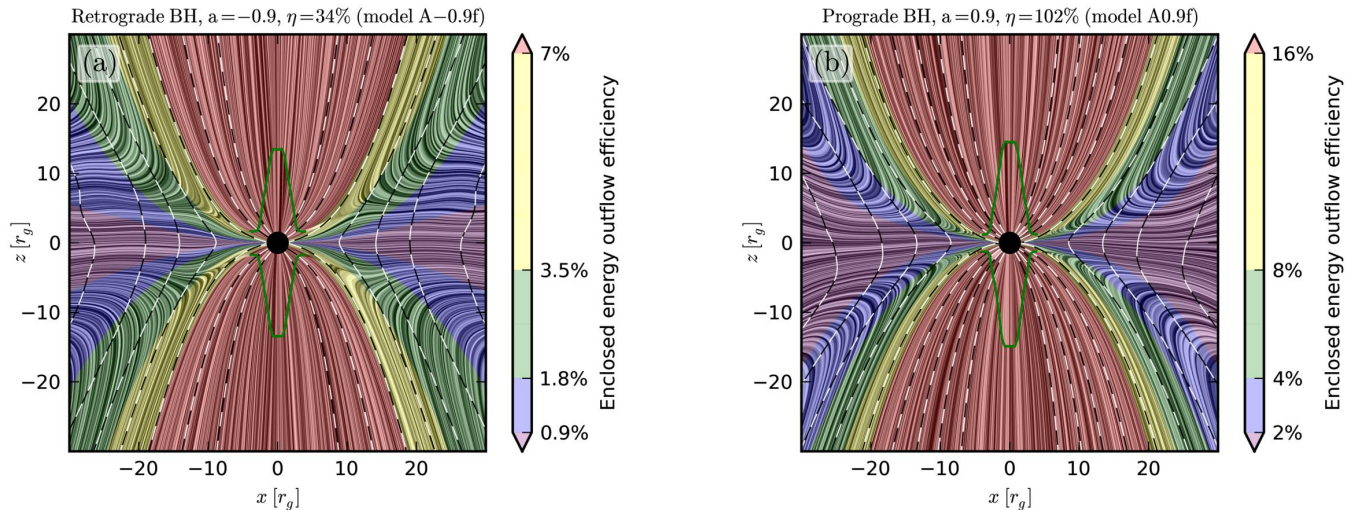


**Figure 3.** Time and azimuthal average flow pattern in our fiducial models, A-0.9f (panel a) and A0.9f (panel b). BH is shown with black filled circle. Black and white dashed lines show poloidal magnetic field lines (constancy levels of dimensionless magnetic flux,  $\phi = \{10, 20, 30, \dots\}$ ). Gray shading shows velocity streamlines. Green lines show the position of stagnation surface, at which  $u^r = 0$ . Colour shows energy outflow efficiency enclosed between the point in question and an equatorial energy flow streamline (see colour bar), so the edges of colour bands represent energy flow streamlines. The flow pattern is a standard hourglass shape: equatorial inflow at low latitudes, inflow-outflow at intermediate latitudes, and twin polar jets (shown in red) at high latitudes.

above values of  $\eta$  to serve as upper bounds on jet efficiency for lower BH spins,  $|a| < 0.9$ , and thinner discs,  $h/r < 0.3$ . We also find that a two-fold increase in disc thickness (to  $h/r \approx 0.6$ ) leads to about a three-fold increase in  $\eta$  (see §2). These results can be used to place limits on the spin of central BHs from the observed values of jet efficiency. However, based on jet energetics alone it will be challenging to tell apart prograde and retrograde BHs due to their similar efficiencies. Future studies should consider radiative effects, which are not included in the current work, and investigate spin-dependence of  $\eta$  for thinner discs, with  $h/r \lesssim 0.1$ .

## ACKNOWLEDGMENTS

AT was supported by a Princeton Center for Theoretical Science Fellowship. AT is grateful to Perimeter Institute for hospitality. We thank A. Broderick, D. Caprioli, I. Contopoulos, D. Giannios, L. Lehner, M. Lyutikov, R. Narayan, R. Nemmen, D. Proga, J. Steiner, J. Stone, and D. Uzdensky for fruitful discussions. We thank the referee, C. Reynolds, for useful suggestions. We acknowledge NSF support via TeraGrid resources: NICS Kraken and Nautilus, where simulations were carried out and data were analyzed, and NCSA MSS and TACC Ranch, where data were backed up, under grant numbers TG-AST100040 (AT) and TG-AST080025N (JCM).

## REFERENCES

- Balbus S. A., Hawley J. F., 1991, *ApJ*, 376, 214  
 Bambi C., 2012, *Phys. Rev. D*, 85, 043002  
 Beckwith K., Hawley J. F., Krolik J. H., 2008, *ApJ*, 678, 1180  
 Bisnovatyi-Kogan G. S., Ruzmaikin A. A., 1974, *Ap&SS*, 28, 45  
 Blandford R. D., Payne D. G., 1982, *MNRAS*, 199, 883  
 Blandford R. D., Znajek R. L., 1977, *MNRAS*, 179, 433  
 Buliga S. D., et al., 2011, *Astrophysics*, 54, 548  
 Cao X., 2011, *ApJ*, 737, 94  
 Chakrabarti S. K., 1985, *ApJ*, 288, 1  
 Daly R. A., 2011, *MNRAS*, 414, 1253  
 De Villiers J.-P., Hawley J. F., 2003, *ApJ*, 589, 458

- Fender R. P., Gallo E., Russell D., 2010, *MNRAS*, 406, 1425  
 Fromang S., Stone J. M., 2009, *A&A*, 507, 19  
 Gammie C. F., McKinney J. C., Tóth G., 2003, *ApJ*, 589, 444  
 Garofalo D., 2009, *ApJ*, 699, 400  
 Garofalo D., Evans D. A., Sambruna R. M., 2010, *MNRAS*, 406, 975  
 Guan X., Gammie C. F., 2009, *ApJ*, 697, 1901  
 Hawley J. F., Guan X., Krolik J. H., 2011, *ApJ*, 738, 84  
 Hawley J. F., Krolik J. H., 2006, *ApJ*, 641, 103  
 Igumenshchev I., Narayan R., Abramowicz M., 2003, *ApJ*, 592, 1042  
 Igumenshchev I. V., 2008, *ApJ*, 677, 317  
 Komissarov S. S., 2001, *MNRAS*, 326, L41  
 Lee H. K., Wijers R. A. M. J., Brown G. E., 2000, *Phys. Rep.*, 325, 83  
 Lei W.-H., Zhang B., 2011, *ApJ*, 740, L27  
 Lesur G., Longaretti P.-Y., 2009, *A&A*, 504, 309  
 Lubow S. H., Papaloizou J. C. B., Pringle J. E., 1994, *MNRAS*, 267, 235  
 Martínez-Sansigre A., Rawlings S., 2011, *MNRAS*, 414, 1937  
 McKinney J. C., 2005, *ApJ*, 630, L5  
 McKinney J. C., Blandford R. D., 2009, *MNRAS*, 394, L126  
 McKinney J. C., Gammie C. F., 2004, *ApJ*, 611, 977  
 McKinney J. C., Tchekhovskoy A., Blandford R., 2012, [arXiv:1201.4163](https://arxiv.org/abs/1201.4163)  
 Narayan R., Igumenshchev I. V., Abramowicz M. A., 2003, *PASJ*, 55, L69  
 Narayan R., McClintock J. E., 2012, *MNRAS*, 419, L69  
 Penna R. F., et al., 2010, *MNRAS*, 408, 752  
 Reynolds C. S., Garofalo D., Begelman M. C., 2006, *ApJ*, 651, 1023  
 Rothstein D. M., Lovelace R. V. E., 2008, *ApJ*, 677, 1221  
 Sorathia K. A., et al., 2011, [ArXiv:1106.4019](https://arxiv.org/abs/1106.4019)  
 Spruit H. C., Uzdensky D. A., 2005, *ApJ*, 629, 960  
 Stehle R., Spruit H. C., 2001, *MNRAS*, 323, 587  
 Tanabe K., Nagataki S., 2008, *Phys. Rev. D*, 78, 024004  
 Tchekhovskoy A., McKinney J. C., Narayan R., 2007, *MNRAS*, 379, 469  
 Tchekhovskoy A., McKinney J. C., Narayan R., 2009, *ApJ*, 699, 1789  
 Tchekhovskoy A., Narayan R., McKinney J. C., 2010, *ApJ*, 711, 50  
 Tchekhovskoy A., Narayan R., McKinney J. C., 2011, *MNRAS*, 418, L79

## SUPPORTING INFORMATION

Additional Supporting Information may be found in the online version of this article:

**Movie files.** Movies of models A-0.9f and A0.9f (click for movies).